5792 *Chem. Mater.* **2009,** *21,* 5792–5800
DOI:10.1021/cm902164t

CHEMISTRY OF MATERIALS
Article

Ethenylene-Bridged Periodic Mesoporous Organosilicas: From *E* to *Z*

Carl Vercaemst,*,† Matthias Ide,† Paul V. Wiper,‡ James T. A. Jones,‡ Yaroslav Z. Khimyak,‡ Francis Verpoort,† and Pascal Van Der Voort*,†

†*Department of Inorganic and Physical Chemistry, Centre for Ordered Materials, Organometallics and Catalysis (COMOC), University of Ghent, Krijgslaan 281, Building S3, 9000 Ghent, Belgium and* ‡*Department of Chemistry, University of Liverpool, Crown Street, Liverpool L69 72D, United Kingdom*

Received July 16, 2009. Revised Manuscript Received October 27, 2009

A novel class of periodic mesoporous organosilicas with *E*- and/or *Z*-configured ethenylene bridges was prepared under acidic conditions using the triblock copolymer Pluronic P123 as a structure directing agent. The isomeric configuration of the precursor has a drastic effect on the properties of the resulting PMO materials. The diastereoisomerically pure *E*-configured ethenylene bridged PMOs reveal higher structural ordering, narrower pore size distributions, and enhanced hydrothermal stability than their diastereoisomerically impure counterparts. These properties have been correlated with the molecular level structure of pore walls probed by solid-state NMR spectroscopy.

Introduction

With the discovery of ordered mesoporous M41S silica materials, synthesized by means of the liquid crystal templating method, a new era in the field of porous materials commenced.[1] Within the next decade, numerous publications on ordered mesoporous materials followed, concerning both the synthesis of novel ordered materials[2,3] and the development of various potential applications in catalysis,[4−6] adsorption chemistry,[7] chromatography,[8−10] environmental technology,[11−13] microelectronics,[14] drug delivery,[15] and sensing.[16−18] A very interesting breakthrough was the discovery of periodic mesoporous organosilicas (PMOs) in 1999.[3,19,20] These novel organic−inorganic hybrid composites are synthesized using bridged organosilanes, most commonly of the type $(R'O)_3Si\text{-}R\text{-}Si(OR')_3$, in the presence of a structure-directing agent (SDA). They are a promising class of ordered materials that combine the structural features of ordered mesoporous silicas with the chemical functionality of organic groups. Doing so, they open up a wide range of new opportunities in designing materials with novel organic functionalities and controlled morphological, structural, and surface properties. To date, PMOs with various rigid organic functionalities have been synthesized, ranging from short aliphatic and aromatic groups such as methane,[21] ethane,[22] ethene,[3,23−27] benzene,[28−30] and xylene[31] to cyclic[32]

*Corresponding author. E-mail: carl.vercaemst@ugent.be (C.V.); pascal.vandervoort@ugent.be (P.V.D.V). Fax: +32 9264 4983. Tel: +32 9264 4442.

(1) Kresge, C. T.; Leonowicz, M. E.; Roth, W. J.; Vartuli, J. C.; Beck, J. S. *Nature* **1992**, *359*, 710.
(2) Zhao, D. Y.; Feng, J. L.; Huo, Q. S.; Melosh, N.; Fredrickson, G. H.; Chmelka, B. F.; Stucky, G. D. *Science* **1998**, *279*, 548.
(3) Asefa, T.; MacLachan, M. J.; Coombs, N.; Ozin, G. A. *Nature* **1999**, *402*, 867.
(4) Corma, A.; Das, D.; Garcia, H.; Leyva, A. *J. Catal.* **2005**, *229*, 322.
(5) Corma, A.; Garcia, H. *Adv. Synth. Catal.* **2006**, *348*, 1391.
(6) Taguchi, A.; Schuth, F. *Microporous Mesoporous Mater.* **2005**, *77*, 1.
(7) Yoshitake, H.; Yokoi, T.; Tatsumi, T. *Chem. Mater.* **2002**, *14*, 4603.
(8) Ma, Y. R.; Qi, L. M.; Ma, J. M.; Wu, Y. Q.; Liu, O.; Cheng, H. M. *Colloids Surf., A* **2003**, *229*, 1.
(9) Martin, T.; Galarneau, A.; Di Renzo, F.; Brunel, D.; Fajula, F.; Heinisch, S.; Cretier, G.; Rocca, J. L. *Chem. Mater.* **2004**, *16*, 1725.
(10) Nassivera, T.; Eklund, A. G.; Landry, C. C. *J. Chromatogr., A* **2002**, *973*, 97.
(11) Fryxell, G. E.; Liu, J.; Hauser, T. A.; Nie, Z. M.; Ferris, K. F.; Mattigod, S.; Gong, M. L.; Hallen, R. T. *Chem. Mater.* **1999**, *11*, 2148.
(12) Liu, A. M.; Hidajat, K.; Kawi, S.; Zhao, D. Y. *Chem. Commun.* **2000**, 1145.
(13) Zhang, L. X.; Zhang, W. H.; Shi, J. L.; Hua, Z.; Li, Y. S.; Yan, J. *Chem. Commun.* **2003**, 210.
(14) Wu, C. G.; Bein, T. *Science* **1994**, *264*, 1757.
(15) Mal, N. K.; Fujiwara, M.; Tanaka, Y. *Nature* **2003**, *421*, 350.
(16) Descalzo, A. B.; Jimenez, D.; Marcos, M. D.; Martinez-Manez, R.; Soto, J.; El Haskouri, J.; Guillem, C.; Beltran, D.; Amoros, P.; Borrachero, M. V. *Adv. Mater.* **2002**, *14*, 966.
(17) Descalzo, A. B.; Rurack, K.; Weisshoff, H.; Martinez-Manez, R.; Marcos, M. D.; Amoros, P.; Hoffmann, K.; Soto, J. *J. Am. Chem. Soc.* **2005**, *127*, 184.
(18) Johnson-White, B.; Zeinali, M.; Shaffer, K. M.; Patterson, C. H.; Charles, P. T.; Markowitz, M. A. *Biosens. Bioelectron.* **2007**, *22*, 1154.
(19) Inagaki, S.; Guan, S.; Fukushima, Y.; Ohsuna, T.; Terasaki, O. *J. Am. Chem. Soc.* **1999**, *121*, 9611.
(20) Melde, B. J.; Holland, B. T.; Blanford, C. F.; Stein, A. *Chem. Mater.* **1999**, *11*, 3302.
(21) Asefa, T.; MacLachlan, M. J.; Grondey, H.; Coombs, N.; Ozin, G. A. *Angew. Chem., Int. Ed.* **2000**, *39*, 1808.
(22) Sayari, A.; Yang, Y. *Chem. Commun.* **2002**, 2582.
(23) Vercaemst, C.; Friedrich, H.; de Jongh, P. E.; Neimark, A. V.; Goderis, B.; Verpoort, F.; Van Der Voort, P. *J. Phys. Chem. C* **2009**, *113*, 5556.
(24) Vercaemst, C.; Ide, M.; Allaert, B.; Ledoux, N.; Verpoort, F.; Van der Voort, P. *Chem. Commun.* **2007**, 2261.
(25) Wang, W. H.; Xie, S. H.; Zhou, W. Z.; Sayari, A. *Chem. Mater.* **2004**, *16*, 1756.
(26) Xia, Y. D.; Yang, Z. X.; Mokaya, R. *Chem. Mater.* **2006**, *18*, 1141.
(27) Vercaemst, C.; de Jongh, P. E.; Meeldijk, J. D.; Goderis, B.; Verpoort, F.; Van Der Voort, P. *Chem. Commun.* **2009**, 4052.
(28) Inagaki, S.; Guan, S.; Ohsuna, T.; Terasaki, O. *Nature* **2002**, *416*, 304.
(29) Kapoor, M. P.; Inagaki, S.; Ikeda, S.; Kakiuchi, K.; Suda, M.; Shimada, T. *J. Am. Chem. Soc.* **2005**, *127*, 8174.
(30) Kuroki, M.; Asefa, T.; Whitnal, W.; Kruk, M.; Yoshina-Ishii, C.; Jaroniec, M.; Ozin, G. A. *J. Am. Chem. Soc.* **2002**, *124*, 13886.
(31) Temtsin, G.; Asefa, T.; Bittner, S.; Ozin, G. A. *J. Mater. Chem.* **2001**, *11*, 3202.
(32) Landskron, K.; Hatton, B. D.; Perovic, D. D.; Ozin, G. A. *Science* **2003**, *302*, 266.

 Published on Web 11/16/2009

and dendritic[33] building blocks. The majority of the literature reports on PMOs though, have been focused on the synthesis of ordered mesoporous ethane silicas, probably because of the wide commercial availability of its precursor 1,2-bis(triethoxysilyl)ethane. As the functional groups of PMOs are homogeneously embedded inside the channel walls, the pore channels are easily accessible for further modification. From this perspective, ethenylene-bridged PMOs are very interesting, as they offer plenty of opportunities for further surface modification based on olefin chemistry.[34−36] To date, ethenylene-bridged PMOs have been synthesized using 1,2-bis(triethoxysilyl)ethene that was either obtained commercially or synthesized according to a method described by Marciniec et al.[37] In either case, the PMO precursor consists of a mixture of two isomers (*E* and *Z* diastereoisomers).

In this contribution, the synthesis of the diastereoisomerically pure *E*-isomer and *Z*-isomer of 1,2-bis(triethoxysilyl)ethene and the development of diastereoisomerically pure *E*- and *Z*-configured ethenylene-bridged PMOs (*E*-EBP and *Z*-EBP, respectively), using the triblock copolymer P123 as a SDA, are presented. We describe the influence of the diastereoisomeric configuration of the PMO precursor on the PMO properties.

Experimental Section

Materials. Vinyltriethoxysilane (VTES), Grubbs' and Hoveyda−Grubbs' first and second generation, $RuCl_2(PPh_3)_3$, [Ru(*p*-cymene)Cl_2]$_2$, and Pluronic P123 ($EO_{20}PO_{70}EO_{20}$) were obtained from Aldrich.

Classic Synthesis of 1,2-bis(triethoxysilyl)ethene. 1,2-Bis(triethoxysilyl)ethene (BTSE) was prepared via metathesis of VTES with $RuCl_2(PPh_3)_3$, according to a method described by Marciniec et al.[37] In a typical synthesis, $RuCl_2(PPh_3)_3$ (0.051 g, 0.053 mmol) and VTES (10.086 g, 0.053 mol) were added to a Schlenk flask under argon. After the solution was stirred and refluxed for 24 h, unreacted VTES was distilled off. Subsequently, BTSE was vacuum distilled to give a clear colorless liquid. Yield: 6.25 g (67%). BTSE was identified by ^{1}H and ^{13}C NMR and GC-analysis as a diastereoisomeric mixture (∼80% *E*), and will be denoted further on in the text as 80(*E*,*Z*)-BTSE. ^{1}H NMR ($CDCl_3$): δ 6.77 (s, 2 H; *Z*-isomer), 6.66 (s, 2 H; *E*-isomer), 3.84 (m, 12 H; *Z*- and *E*-isomer), 1.23 ppm (t, 18 H; *Z*-and *E*-isomer). ^{13}C NMR ($CDCl_3$): δ 151.42 (*Z*-isomer), 145.92 (*E*-isomer), 58.82 (*E*-isomer), 58.71 (*Z*-isomer), 18.45 (*E*-isomer), 18.40 ppm (*Z*-isomer).

Direct Synthesis of the Diastereoisomerically Pure *E*-Isomer of 1,2-Bis(triethoxysilyl)ethene. For the synthesis of the diastereoisomerically pure *E*-isomer of 1,2-bis(triethoxysilyl)ethene (*E*-BTSE), the Grubbs' first-generation catalyst was used, according to a procedure recently reported by our group.[24] In a typical synthesis of *E*-BTSE, $(PCy_3)_2Cl_2Ru{=}CHPh$ (0.0535 g, 0.065 mmol) and VTES (42.95 mL, 0.2038 mol) were added to a Schlenk flask under argon. The mixture was left to stir for 1 h and subsequently refluxed for an additional 3 h. Unreacted VTES was distilled off, after which *E*-BTSE was vacuum distilled to give a clear colorless liquid. Yield: 33.8 g (94%). *E*-BTSE was identified by ^{1}H and ^{13}C NMR and GC-analysis as a diastereoisomerically pure product (∼100% *E*). ^{1}H NMR ($CDCl_3$): δ 6.63 (s, 2 H), 3.84 (q, 12 H), 1.23 ppm (t, 18 H). ^{13}C NMR ($CDCl_3$): δ 145.92, 58.82, 18.45 ppm.

Synthesis of Diastereoisomeric Mixture and Diastereoisomerically Pure *Z*-Isomer of 1,2-Bis(triethoxysilyl)ethene. Both the diastereoisomeric mixture (50% *E*) of 1,2-bis(triethoxysilyl)ethene (abbreviated as 50(*E*,*Z*)-BTSE) and the pure *Z*-isomer of 1,2-bis(triethoxysilyl)ethene (*Z*-BTSE) were prepared via successive fractionated vacuum distillations of 80(*E*,*Z*)-BTSE. The distillation was monitored with ^{1}H NMR and GC to obtain a clear colorless liquid with the desired isomeric purity. ^{1}H NMR of *Z*-BTSE ($CDCl_3$): δ 6.76 (s, 2 H), 3.86 (q, 12 H), 1.23 ppm (t, 18 H). ^{13}C NMR of *Z*-BTSE ($CDCl_3$): δ 151.37, 58.70, 18.39 ppm.

Preparation of Ethenylene-Bridged Periodic Mesoporous Organosilicas. A series of PMOs was synthesized by varying the precursor and keeping all other reaction parameters constant. In a typical synthesis procedure, 1.00 g of Pluronic P123 was diluted in an acidified solution containing 47.80 mL of H_2O, 3.42 mL of concentrated HCl, and 2.45 mL of n-butanol. The solution was stirred at room temperature for 1.5 h, upon which 1.86 mL of *E*-BTSE, *Z*-BTSE, 50(*E*,*Z*)-BTSE, or 80(*E*,*Z*)-BTSE was added. The final reactant molar composition was 1:29:238:16097:155 P123:BTSE:HCl:H_2O:BuOH. This solution was stirred for 4 h at 35 °C, upon which 18.0 mL of n-butanol was added. The PMO material was successively aged for an additional 23 h at 90 °C under static conditions. The mixture was left to cool to room temperature, after which the precipitated PMO was filtrated and washed with distilled water. The surfactant was removed by means of Soxhlet extraction using acetone over a period of 5 h. This procedure led to ethenylene-bridged hybrid materials with different isomeric configurations. Throughout the text, the diastereoisomerically pure *E*-configured and *Z*-configured ethenylene-bridged PMOs are denoted as *E*-EBP and *Z*-EBP, respectively, whereas 80(*E*,*Z*)-EBP and 50(*E*,*Z*)-EBP refer to PMOs consisting of 80% *E*-isomer (20% *Z*-isomer) and 50% *E*-isomer (50% *Z*-isomer), respectively. Disordered *Z*-configured ethenylene-bridged organosilicas are abbreviated as *Z*-EBO. For the synthesis of *Z*-EBP, 8.9 mL of concentrated HCl was used, while keeping all other reaction parameters constant.

Hydrothermal Treatment. The PMO materials were brought onto a small grid in an autoclave containing distilled H_2O. The temperature was raised to 105 °C at which the materials were steamed for 24 h under autogenous pressure. The resulting materials were vacuum-dried at 110 °C overnight.

Bromination of Ethenylene-Bridged PMOs. The accessibility of the C=C double bonds in the ethene-PMOs was investigated by means of a bromine addition reaction. The PMOs were treated with bromine vapor under vacuum at 35 °C. The reaction time was varied (0.5, 1, 2, and 6 h). Physisorbed bromine was removed under a vacuum at 90 °C.

Characterization. X-ray powder diffraction (XRD) patterns were collected on a Siemens D5000 Diffractometer with Cu Kα radiation with 0.15418 nm wavelength.

Nitrogen adsorption experiments were performed at 77 K using a Belsorp-mini II gas analyzer. Samples were vacuum-dried overnight at 90 °C prior to analysis. The specific surface

(33) Landskron, K.; Ozin, G. A. *Science* **2004**, *306*, 1529.
(34) Vercaemst, C.; Jones, J. T. A.; Khimyak, Y. Z.; Martins, J. C.; Verpoort, F.; Van der Voort, P. *Phys. Chem. Chem. Phys.* **2008**, *10*, 5349.
(35) Nakai, K.; Oumi, Y.; Horie, H.; Sano, T.; Yoshitake, H. *Microporous Mesoporous Mater.* **2007**, *100*, 328.
(36) Nakajima, K.; Tomita, I.; Hara, M.; Hayashi, S.; Domen, K.; Kondo, J. N. *Catal. Today* **2006**, *116*, 151.
(37) Marciniec, B.; Maciejewski, H.; Gulinski, J.; Rzejak, L. *J. Organomet. Chem.* **1989**, *362*, 273.

Scheme 1. Investigated Catalysts in the Olefin Self-Metathesis Reaction of VTES

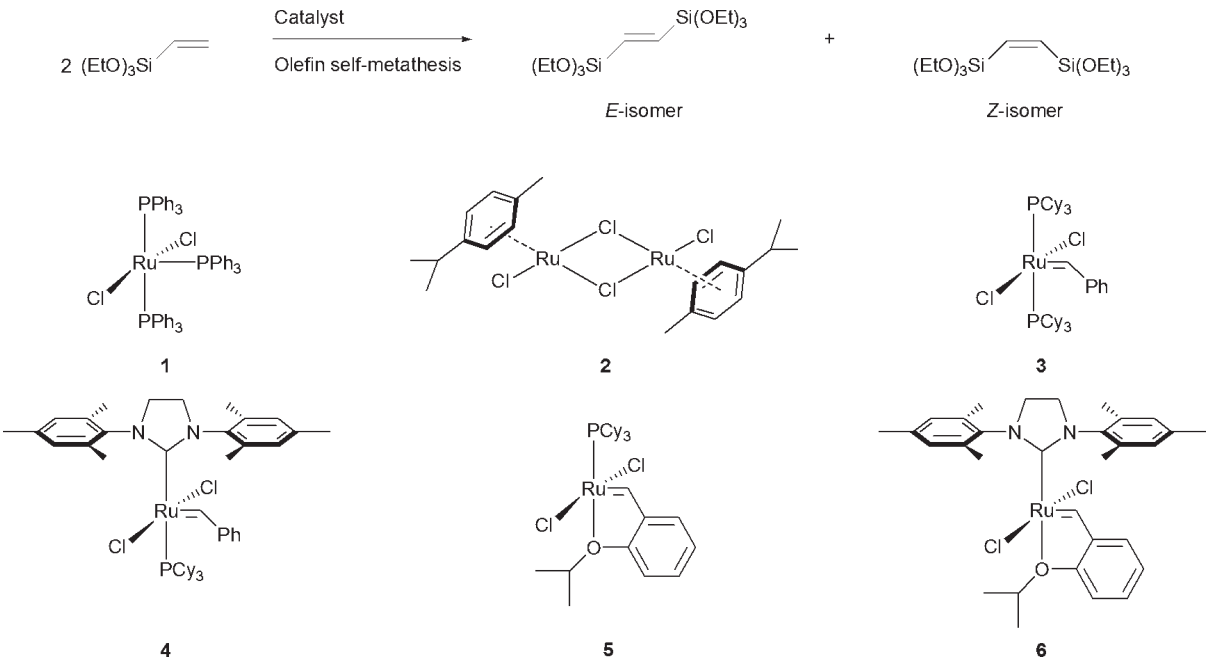

area, S, was determined from the linear part of the BET plot (P/P_0 = 0.05−0.15). The total pore volume, V_t, was determined from the amount of nitrogen adsorbed at P/P_0 = 0.98, while the micropore volume, V_μ, was calculated by the *t*-plot method (P/P_0 = 0.31−0.51). The pore size distribution, PSD, was calculated from the adsorption branch using the BJH method. The pore-wall thickness, t_w, was estimated using the equation $t_w = (a_0 - D_p)$, where a_0 and D_p are the unit cell dimension and pore size, respectively.

FT-Raman spectra were acquired on an Equinox 55S hybrid FT-IR/FT-Raman spectrometer with a Raman module FRA 106 from Bruker. The spectrometer is fitted with a N_2-cooled germanium high-sensitivity detector D418-T and a N_2-cooled MCT-B detector. The Raman laser wavelength is the 1064 nm line of an air cooled diode pumped neodymium yttrium aluminum garnet laser (Nd:YAG). The laser power was manually set to 300 mW.

The ^{1}H and ^{13}C solution NMR spectra were collected on a Varian Unity-300 spectrometer. GC analysis was conducted on a Finnigan Trace GC ultra GC equipped with a standard FID detector. A wall-coated open tubular column with a length of 10 m, an internal diameter of 0.10 mm, and a coating of 0.40 μm (5% diphenyl and 95% dimethyl polysiloxane) was used.

All solid-state NMR experiments were conducted at 9.4 T using a Bruker DSX-400 spectrometer operating at 79.49, 100.61, and 400.13 MHz for ^{29}Si, ^{13}C, and ^{1}H, respectively. All chemical shifts are quoted in ppm from external TMS. ^{1}H−^{13}C CP/MAS NMR spectra were acquired at a MAS rate of 8.0 kHz. A ^{1}H $\pi/2$ pulse length was 3.0 μs and a recycle delay of 8.0 s was used during acquisition. The CP contact time was 2.0 ms with the Hartmann−Hahn matching condition set using Hexamethylbenzene (HMB). ^{1}H−^{13}C Variable Contact Time (VCT) CP/MAS NMR spectra were acquired using contact times in the range of 0.01 to 12.0 ms. ^{1}H−^{29}Si CP/MAS NMR spectra were acquired at a MAS rate of 4.0 kHz. A ^{1}H $\pi/2$ pulse length of 3.1 μs and the recycle delay of 10 s was used during acquisition. The CP contact time was 2.0 ms with the Hartmann−Hahn matching condition set using kaolinite. The ^{1}H−^{29}Si VCT/CP MAS NMR measurements used contact times ranging from 0.05 to 16.0 ms. 2D ^{1}H−^{13}C wideline separation (WISE) MAS NMR spectra were acquired at a MAS rate of 8 kHz. The ^{1}H $\pi/2$ pulse length was 3.1 μs TPPM decoupling with a rf field strength of 84.7 kHz was used during the acquisition in t_2. The Hartmann−Hahn condition was set using HMB. A fixed contact time of 80 μs was used to limit the effect of spin diffusion. Longer contact times would lead to an equilibration of the proton magnetization due to spin diffusion, and consequently to the same proton line shape for all carbon sites.[38] States for phase-sensitive detection in the indirect dimension was implemented to recover pure absorption line shape. The recycle time was 2 s. 256 increments were recorded in t_1 corresponding to a dwell time of 16.7 μs at a spectral width of 59880.238 Hz. 496 transients were acquired per t_1 increment in the direct dimension.

Results and Discussion

Precursor Synthesis and Role of Catalyst. The synthesis of 1,2-bis(triethoxysilyl)ethene proceeds by means of an olefin self-metathesis reaction of VTES, as depicted in Scheme 1. In our effort to catalytically obtain the pure *E*-isomer of 1,2-bis(triethoxysilyl)ethene, were probed several catalysts, illustrated in Scheme 1. Table 1 gives the investigated catalysts and their selectivity in the metathesis of VTES.

The commercially available Grubbs' first-generation catalyst **3**, is the most selective catalyst. The latter produced the pure *E*-diastereoisomer of 1,2-bis(triethoxysilyl)ethene, without further purification being necessary. Catalyst **1**, the commonly applied catalyst for the metathesis of VTES, produced a diastereoisomeric mixture containing about 79.7% of the *E*-isomer.

The diastereoisomeric configuration of *E*-BTSE is maintained in the final PMO-material, *E*-EBP, as evidenced by FT-Raman and ^{1}H−^{13}C CP/MAS NMR spectroscopy.

(38) Clauss, J.; Schmidtrohr, K.; Adam, A.; Boeffel, C.; Spiess, H. W. *Macromolecules* **1992**, *25*, 5208.

Table 1. Diastereoselectivity of the Investigated Catalysts for *E*-BTSE

catalyst	diastereoselectivity (% *E*)[a]
Grubbs' 2nd generation, **4**	79.3
$RuCl_2(PPh_3)_3$, **1**	79.7
$[Ru(p\text{-cymene})Cl_2]_2$, **2**	89.2
Hoveyda−Grubbs' 2nd generation, **6**	92.1
Hoveyda−Grubbs' 1st generation, **5**	94.6
Grubbs' 1st generation, **3**	∼100

[a] Determined via GC analysis.

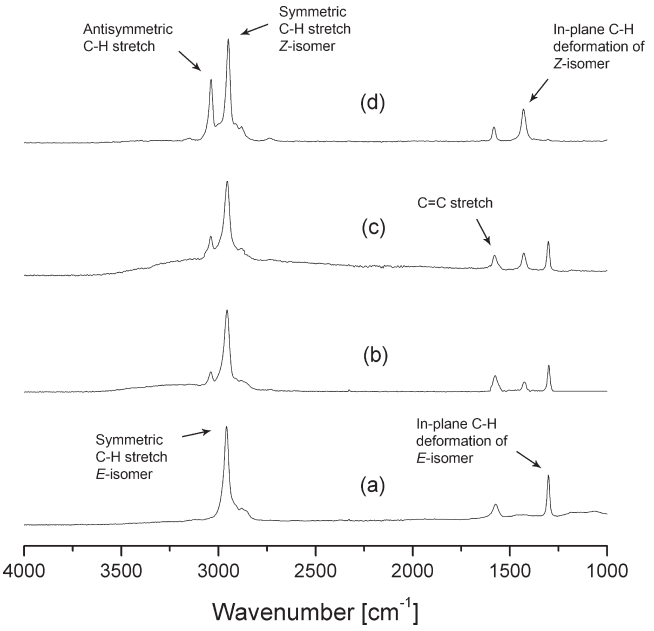

Figure 1. FT-Raman spectra of (a) *E*-EBP, (b) 80(*E*,*Z*)-EBP, (c) 50(*E*, *Z*)-EBP, and (d) *Z*-EBO.

The FT-Raman spectra of (a) *E*-EBP (100% *E*), and (b) 80(*E*,*Z*)-EBP (∼80% *E*), are given in Figure 1.

Both Raman spectra exhibit intense peaks at 2956, 1575, and 1301 cm^{-1}. These peaks can be assigned to the C−H stretch vibration, the C═C stretch vibration and the in-plane C−H deformation of the *E*-isomer, respectively. The peaks at 3039 and 1428 cm^{-1}, visible in spectrum (b), can be assigned to the *Z*-isomer. Comparison of spectra (a) and (b) clearly shows that *E*-EBP consists of only *E*-configured ethenylene bridges.

Overall, the final diastereoisomeric ratio of 1,2-bis-(triethoxysilyl)ethene is under thermodynamic control, with relatively unhindered triethoxy groups in *E*-configuration and more hindered triethoxy groups in *Z*-configuration. This rationalizes the high selectivity of the described catalysts for the *E*-isomer. In other words, to obtain a lower *E*/*Z* ratio, a different synthesis approach is required. As the *Z*-isomer of 1,2-bis(triethoxysilyl)ethene has a slightly lower boiling point than the *E*-isomer, the *E*/*Z* ratio can be lowered by performing multiple successive fractionated vacuum distillations. This way, the amount of *Z*-isomer can be varied from 20 to 100%. According to this method both 50(*E*,*Z*)-BTSE, which consists 50% of both the *E*- and *Z*-isomers, and *Z*-BTSE, which is the 100% pure *Z*-diastereoisomer of 1,2-bis(triethoxysilyl)ethene, were synthesized. These two precursors were employed in the synthesis of the corresponding hybrid materials, 50(*E*,*Z*)-EBP and *Z*-EBO. In Figure 1, the FT-Raman spectra of (c) 50(*E*, *Z*)-EBP and (d) *Z*-EBO are given, respectively. The Raman spectrum of *Z*-EBO exhibits intense peaks at 3038, 2949, 1582, and 1430 cm^{-1}. These peaks can be assigned to the antisymmetric and symmetric C−H stretch, the C═C stretch and the in-plane C−H deformation of the *Z*-configured ethenylene bridges, respectively.

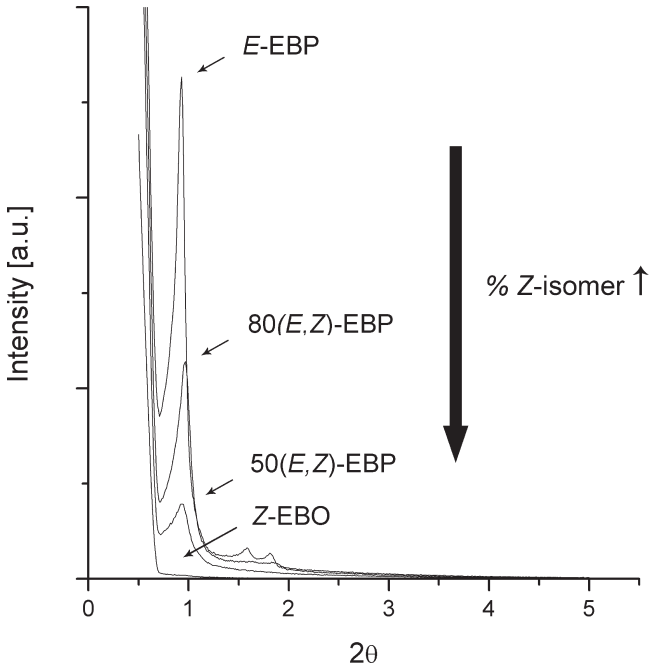

Figure 2. XRD plots of *E*-EBP, 80(*E*,*Z*)-EBP, 50(*E*,*Z*)-EBP, and *Z*-EBO.

Influence of Isomeric Configuration on PMO Structural Properties. The isomeric configuration of 1,2-bis-(triethoxysilyl)ethene plays a significant role in the ordering of the ethenylene-briged PMOs, as illustrated by the XRD-patterns in Figure 2. *E*-EBP has a much better ordering than 80(*E*,*Z*)-EBP and 50(*E*,*Z*)-EBP. *E*-EBP reveals three well-resolved peaks that can be attributed to the (100), (110), and (200) reflections. These assignments are consistent with a hexagonally ordered material with a *P6mm* space group. 80(*E*,*Z*)-EBP on the other hand, only reveals one peak which can be attributed to the (100) reflection of the 2D hexagonal unit cell. The intensity of the (100) reflection further decreases with increasing amount of *Z*-isomer.

In Figure 3, the nitrogen isotherms and the BJH pore size distributions of *E*-EBP, 80(*E*,*Z*)-EBP, 50(*E*,*Z*)-EBP, and *Z*-EBO are given. Distinctive features of these organosilicas are the capillary condensation and evaporation steps in the nitrogen isotherms. These are almost vertical in the case of *E*-EBP, whereas for 80(*E*,*Z*)-EBP, these are far less steep. In fact, with increasing amount of *Z*-isomer, the inclinations of the capillary condensation and evaporation steps decrease. This reflects in the much narrower pore size distribution of *E*-EBP when compared to that of 80(*E*,*Z*)-EBP and 50(*E*,*Z*)-EBP.

When *Z*-BTSE is used as a precursor under the given reaction conditions, a microporous material is obtained. These results suggest that the *Z*-isomer of

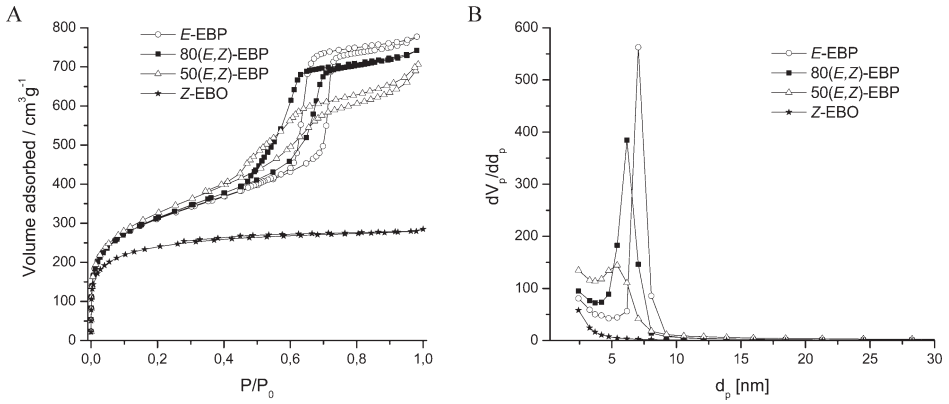

Figure 3. (A) Nitrogen isotherms and (B) BJH pore size distributions of *E*-EBP, 80(*E*,*Z*)-EBP, 50(*E*,*Z*)-EBP, and *Z*-EBO.

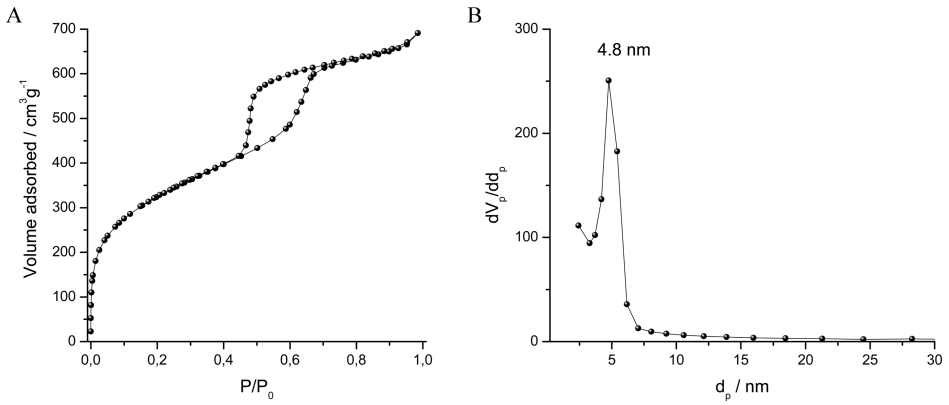

Figure 4. (A) Nitrogen isotherms and (B) BJH pore size distributions of *Z*-EBP.

1,2-bis(triethoxysilyl)ethene has a different reactivity than the *E*-isomer, which has to be taken into account when employing diastereoisomeric mixtures for the synthesis of ethenylene-bridged PMOs.

The enhanced pore ordering and pore size uniformity of *E*-EBP is most probably a result of the homogeneous polycondensation of *E*-BTSE and in particular the more regular cross-linking and stacking of the *E*-configured ethenylene-bridges. In the case of 80(*E*,*Z*)-BTSE and 50(*E*,*Z*)-BTSE, the polycondensation rates of the two isomers are different and the cross-linking and stacking of the ethenylene bridges will proceed at random. Because the described synthesis procedure is optimized for the *E*-isomer of 1,2-bis(triethoxysilyl)ethene, the presence of the *Z*-isomer disturbs the self-assembly which results in an inferior structural ordering and pore size uniformity. This hypothesis is supported by the complete loss of structural ordering when employing *Z*-BTSE as a precursor. The structural ordering and pore uniformity of *Z*-configured ethenylene-bridged PMOs (*Z*-EBP) can be enhanced by altering the reaction conditions. In particular, lowering the pH of the reaction mixture enhances the template/*Z*-BTSE interaction and favors the formation of *Z*-EBP with uniform pores instead of disordered *Z*-EBO. Below, the template/framework interaction will be discussed from an NMR perspective. The nitrogen isotherms and BJH pore size distribution of *Z*-EBP are given in Figure 4. A full characterization of *Z*-EBP is given in the ESI.

The required high acidity for the formation of *Z*-EBP ($\approx$ 2.1 mol/L) when compared to that needed for *E*-EBP ($\approx$ 0.8 mol/L), verifies the significant difference in reactivity between *Z*-BTSE and *E*-BTSE and rationalizes the reduced pore ordering and uniformity of ethenylene-bridged PMOs synthesized from diastereoisomeric mixtures.

In Table 2, the properties of the discussed hybrid materials are given. Besides having a drastic effect on the pore ordering and pore uniformity, the isomeric configuration clearly also has a significant effect on the micropore volume, the pore size, and the pore-wall thickness. The isomeric configuration has little effect on the unit-cell dimension of the PMOs. Consequently, the decrease in pore size with the increasing contribution of *Z*-isomer is related to the increase in the pore-wall thickness. The closer stacking of *E*-isomers in comparison to *Z*-isomers is a known fact that is related to their more linear shape, and rationalizes the increasing pore-wall thickness with increasing content of *Z*-configured ethenylene groups.

Understanding the Local Structure of Ethenylene-Bridged PMOs. The $^{1}H-^{13}C$ CP/MAS NMR spectrum of *E*-EBP (Figure 5) clearly exhibits a single resonance at 146.7 ppm corresponding to the *E*-configured CH=CH− bridging organic groups. The spectrum of *Z*-EBO shows two lines at 150.0 and 138.8 ppm. The spectra of 80(*E*,*Z*)-EBP and 50(*E*,*Z*)-EBP result from the superposition of the lines detected for pure *E*- and *Z*-isomers.

Though the line at 138.8 ppm in the spectra of ethene-PMOs consisting of the *Z*-isomer is unexpected, very

Table 2. Properties of Ethenylene-Bridged Hybrid Materials

sample	% *E*-isomer	% *Z*-isomer	S^a (m^2/g)	V_t^b (cm^3/g)	V_μ^c (cm^3/g)	D_p^d (nm)	a_0^e (nm)	t_w^f (nm)
E-EBP	100	0	1133	1.20	0.18	7.1	11.0	3.9
80(*E,Z*)-EBP	80	20	1144	1.15	0.12	6.2	10.5	4.3
50(*E,Z*)-EBP	50	50	1187	1.09	0.06	5.4	10.8	5.4
Z-EBO	0	100	1143	0.44	0.44	< 2	-	-
Z-EBP	0	100	1160	1.03	0.14	4.8	10.7	6.0

[a] Surface area. [b] Total pore volume. [c] Micropore volume. [d] Pore diameter. [e] Unit-cell dimension. [f] Pore-wall thickness.

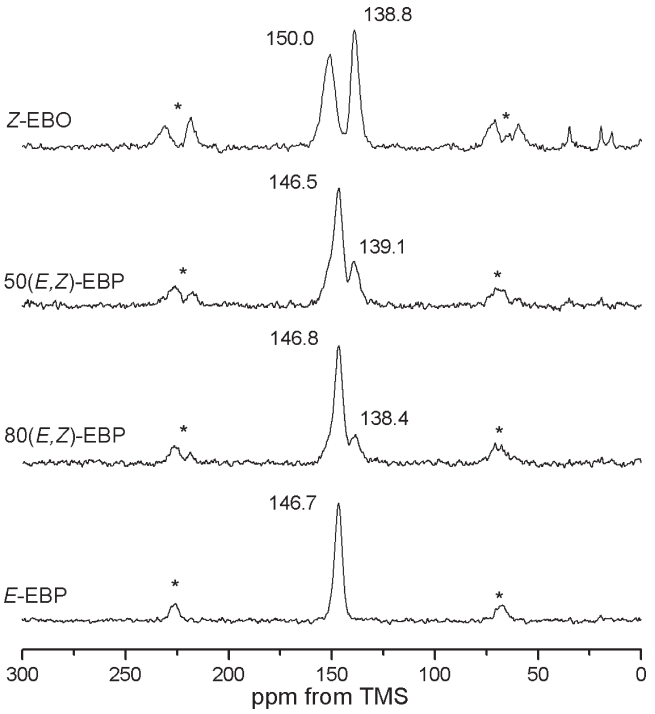

Figure 5. $^1H-^{13}C$ CP/MAS NMR spectra of ethene-PMOs acquired at an MAS rate of 8 kHz using a contact time of 2 ms. Asterisks denote spinning sidebands.

careful examination of the reported solid-state NMR data for typical ethene PMOs (i.e., consisting of both isomers) also indicates the presence of this line, whereas the expected peak at 150 ppm is usually masked by a more intense line from the *E*-isomer at ca. 147 ppm.[25,36,39]

We used the $^1H-^{13}C$ CP kinetics to examine the origin of the second resonance in the spectra of ethenylene-bridged PMOs consisting of the *Z*-isomer (full description of CP-kinetics is given in the ESI). The results of the CP-kinetics for the peaks at 147 ppm for *E*-EBP and at 150 ppm for *Z*-EBP are consistent with our previous observations for framework forming organic bridges.[40,41] Similarly to mono- and bifunctional $-CH_2CH_2-$/$-CH{=}CH-$ PMOs, we note that the $^1H-^{13}C$ CP/MAS kinetics curves give unsatisfactory results when fitted using either classical I−S or a more complex I−I*−S model relaying on the presence of heterogeneous ^1H population. This can be explained only using an approach where two components with different T_{IS} and $T_{1\rho}{}^H$ times are identified depending on the mobility of the CP-determining ^1H source spins. The "rigid" component displays extremely short T_{cp} and $T_{1\rho}{}^H$ times and the "mobile" component shows much longer T_{cp} and $T_{1\rho}{}^H$ times. The fast CP of the rigid components is a result of directly attached protons with reduced mobility and is indicative of a strong $^1H-^{13}C$ heteronuclear dipolar coupled network, thus representing organic bridges embedded in the bulk of hybrid pore walls. The mobile component with slow CP kinetics can be attributed to organic bridges located at the pore-wall interface.

It is important to note that the peak at 138.8 ppm displays much slower CP-kinetics, indicative of ^{13}C sites with no directly attached protons. The CP for such sites relies on ^1H spin-diffusion. The $^1H-^{13}C$ Heteronuclear Correlation (HETCOR) spectrum of *Z*-EBO (see the Supporting Information) shows the same cross-peak pattern for the lines at 150 and 138.8 ppm. This is indicative that two types of ^{13}C species represented by respective lines in the ^{13}C spectra are in close proximity to the same ^1H source, i.e., sp^2 carbon atoms and belong to the same porous network.

The $^1H-^{13}C$ CP/MAS NMR kinetics of as-synthesized ethene-PMOs confirm these observations (the spectra of as-synthesized PMOs are given in the ESI). The framework-forming $-CH{=}CH-$ organic moieties at 146.8 ppm (*E*-isomer) and 150.0 ppm (*Z*-isomer) show the presence of two components with siginificantly different CP-kinetics. Because the ^1H pool is now dominated by the organic template, the $T_{1\rho}{}^H$ times for the mobile component are reduced in comparison with the template extracted materials. The CP-kinetics of the peak at ca. 139 ppm is typical for quaternary carbon sites (see the Supporting Information). Similarly to the other sites, the $T_{1\rho}{}^H$ time is reduced in comparison with the template extracted materials.

The $^1H-^{13}C$ CP/MAS dynamics enabled us to assess the strength of the template/framework interactions. The ^{13}C resonance at ca. 71 ppm attributable to the PEO block of the template shows the fastest CP-kinetics in comparison with the peaks of the PPO blocks ($-OCH_2\underline{C}H(CH_3)-$ at ca. 76 ppm, $-O\underline{C}H_2CH(CH_3)-$ at 74 pm, and a methyl group at ca. 17 ppm). This is indicative of its restricted mobility due to location at the pore interface. The slower CP-kinetics of the peaks corresponding to the PPO blocks is due to their location in the middle of the pores. Such distribution of different blocks of the template is confirmed by the 2D wide-line separation (WISE) spectra of the as-synthesized

(39) Nakajima, K.; Tomita, I.; Hara, M.; Hayashi, S.; Domen, K.; Kondo, J. N. *J. Mater. Chem.* **2005**, *15*, 2362.
(40) Jones, J. T. A.; Wood, C. D.; Dickinson, C.; Khimyak, Y. Z. *Chem. Mater.* **2008**, *20*, 3385.
(41) Treuherz, B. A.; Khimyak, Y. Z. *Microporous Mesoporous Mater.* **2007**, *106*, 236.

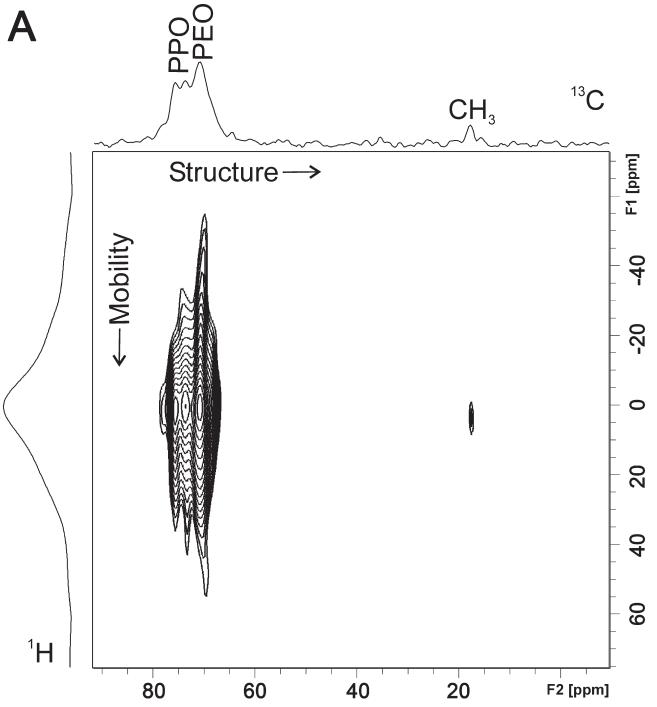

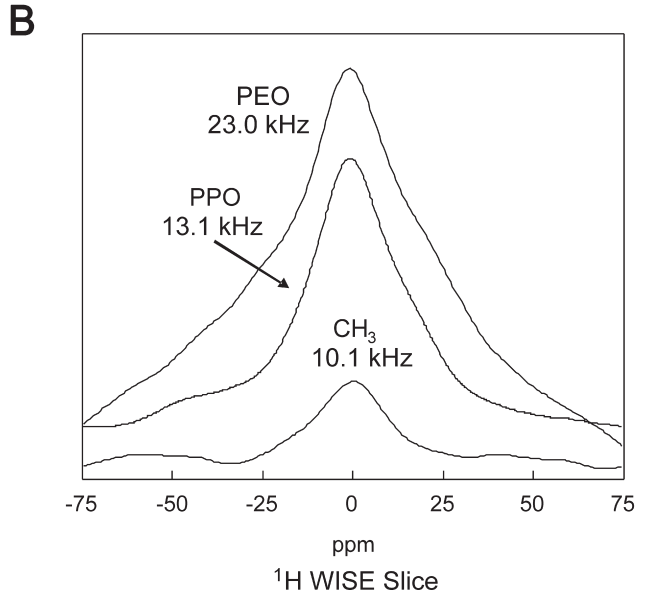

Figure 6. $^{1}H-^{13}C$ WISE NMR spectrum of (A) as-synthesized 80(*E,Z*)-EBP and (B) corresponding ^{1}H projections.

ethene-PMO 80(*E,Z*)-EBP. The $^{1}H-^{13}C$ WISE spectrum (Figure 6A) correlates the ^{13}C spectrum (structure) in the direct dimension with the ^{1}H spectrum (mobility) in the indirect dimension. That is, the ^{1}H line width is dependent upon the mobility with narrower lines observed for increasingly mobile ^{1}H environments. The ^{13}C dimension shows the same template resonances as described in the CP/MAS spectra (Figure 5) correlating to the broad lines in the ^{1}H dimension.

The ^{1}H wide-line corresponding to the PEO block confirms the rigidity of its protons as a line width of 23.0 kHz is observed. However the ^{1}H lines correlating to the ^{1}H PPO environments are significantly narrower than

Scheme 2. Template−Framework Interactions Inferred from the $^{1}H-^{13}C$ CP/MAS Kinetics and WISE Experiments

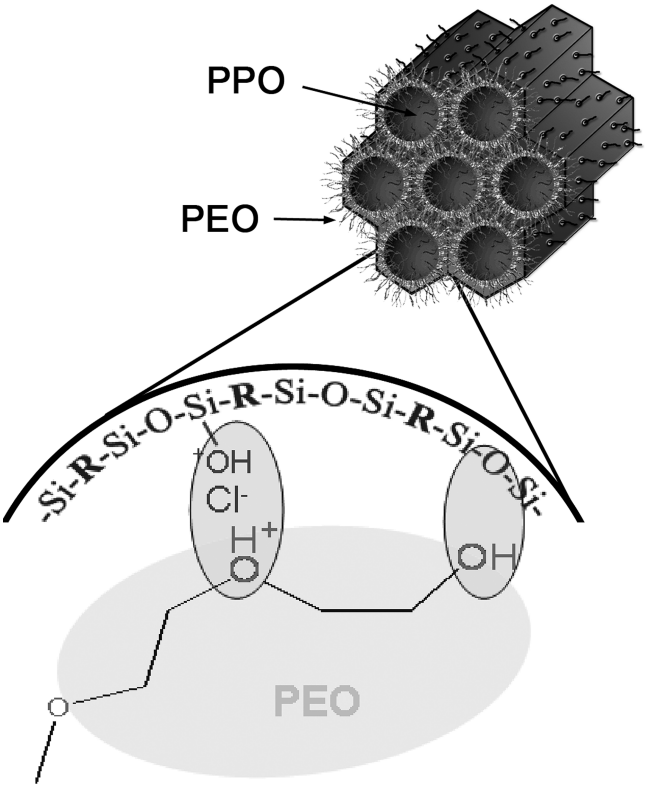

that of the PEO species providing further confirmation that the PPO block is highly mobile within the pores of the mesoporous framework. It is also worthy to note that the ^{1}H projection of the −CH=CH− groups display a broad resonance superimposed on a narrow peak, confirming two different ^{1}H mobility's depending on the location of the functionalities within the framework consistent with $^{1}H-^{13}C$ CP kinetics studies.

The $^{1}H-^{13}C$ CP/MAS kinetics curves and 2D WISE NMR spectra have both provided complementary information on the environments of the template components in as-synthesized ethene-PMOs. The similarity in the CP-kinetics parameters between the as-synthesized well-ordered *Z*- and *E*-configured ethenylene-bridged PMOs is indicative of comparable strength of template/framework interactions leading to materials with similar degree of mesoscopic ordering. The PEO component is strongly interacting with the hybrid pore walls whereas, the PPO block is mobile in the pores (Scheme 2). The interactions between the hybrid walls and the PEO block are H-bonding through terminal PEO −OH groups and the Si−O−Si environments as well as ion-pairing through the halide anion of the protonated ether functionality in the PEO blocks and the $\equiv Si-{}^{+}OH_2$ functionalities as shown in Scheme 2.

Hydrothermal Stability. To investigate the influence of the isomeric configuration of the PMO pore walls on the stability of these materials, *E*-EBP and 80(*E,Z*)-EBP were steamed for 24 h in an autoclave at 105 °C, the results of which are illustrated in Figure 7. 80(*E,Z*)-EBP was chosen as a reference as this sample comes closest (in terms of

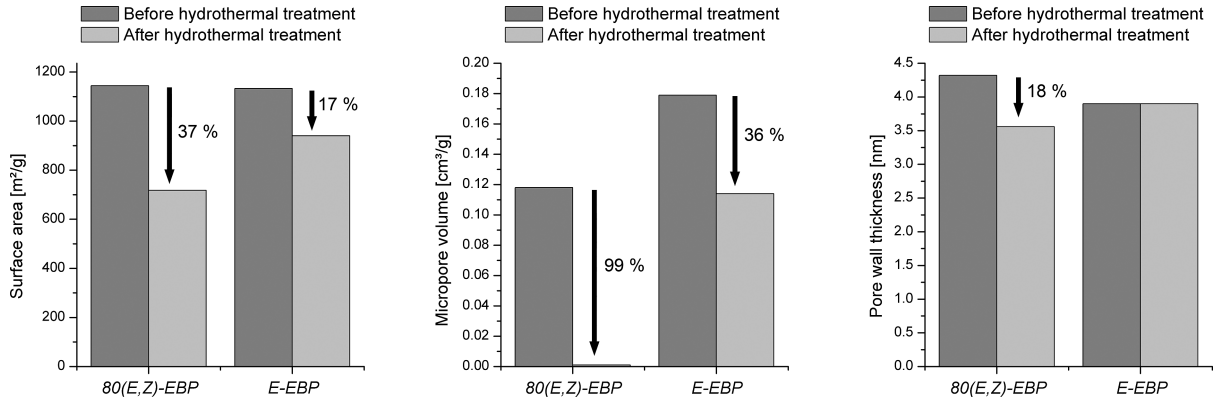

Figure 7. Influence of the isomeric configuration on the hydrothermal stability.

isomeric configuration) to the ethenylene-bridged PMOs that have been reported so far. Clearly, the hydrothermal treatment has a significantly larger negative impact on the properties of 80(*E*,*Z*)-EBP in comparison to *E*-EBP, indicating that the stability of ethenylene-bridged PMOs can be enhanced by employing *E*-BTSE instead of the commonly applied precursor 80(*E*,*Z*)-BTSE. Most interesting is the contraction of the pore walls of 80(*E*,*Z*)-EBP, whereas these of *E*-EBP remain unaffected. This may be explained by the poorer packing of the ethenylene groups in 80(*E*,*Z*)-EBP when compared to *E*-EBP. The contraction of the pore walls after hydrothermal treatment confirms the hypothesis that the increase in the pore wall thickness with increasing amount of *Z*-isomer can be related to the poorer stacking of the *Z*-configured ethenylene bridges compared to that of the *E*-configured ethenylene bridges.

The lower hydrothermal stability of the ethenylene-bridged PMOs containing the *Z*-isomer can also be assigned to the lower condensation degree in the PMO pore walls. The degree of condensation of pore wall was assessed using the $^{1}H-^{29}Si$ CP/MAS kinetics (see the Supporting Information). All PMOs show that the T_{IS} times increase with Si condensation from R-Si(OH)$_2$(OSi) T^1 to R-Si(OSi)$_3$ T^3 environments. This is to be expected because of the protons in the Si−OH moieties facilitating CP "build up". The PMOs containing *Z*-configured CH=CH bridges show no evidence of $T_{1\rho}{}^{H}$ relaxation, suggesting the "proton pool" is sparsely populated and only week $^{1}H-^{1}H$ dipolar coupling is present. *E*-EBP shows a significant $T_{1\rho}{}^{H}$ relaxation, suggesting stronger $^{1}H-^{1}H$ dipolarly coupled network. Therefore, the degree of condensation of the framework was calculated taking into account the differences in $^{1}H-^{29}Si$ CP/MAS kinetics. Thus, the $(T^1 + T^2)/T^3$ ratio is the lowest for *E*-EBP and is much higher for the PMOs consisting of *Z*-configured CH=CH bridges, indicating a more condensed framework in the former. The line widths of ^{29}Si resonances are the largest for the *Z*-EBO (Figure 8).

Chemical Accessibility of the Ethene Functions: Bromination. The chemical accessibility of the PMO ethene functionalities was investigated by means of bromination. Figure 9 gives the FT-Raman spectrum of an ethenylene-bridged PMO (a) before and (b) after bromination. An

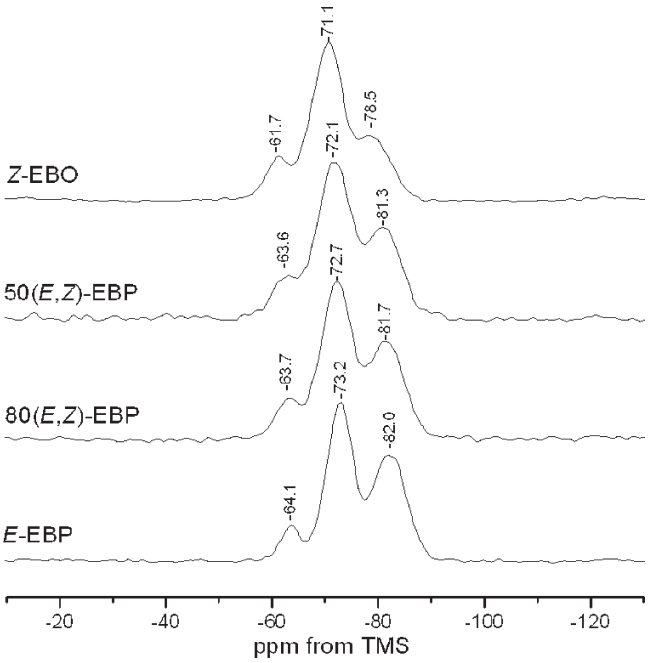

Figure 8. $^{1}H-^{29}Si$ CP/MAS NMR Spectra.

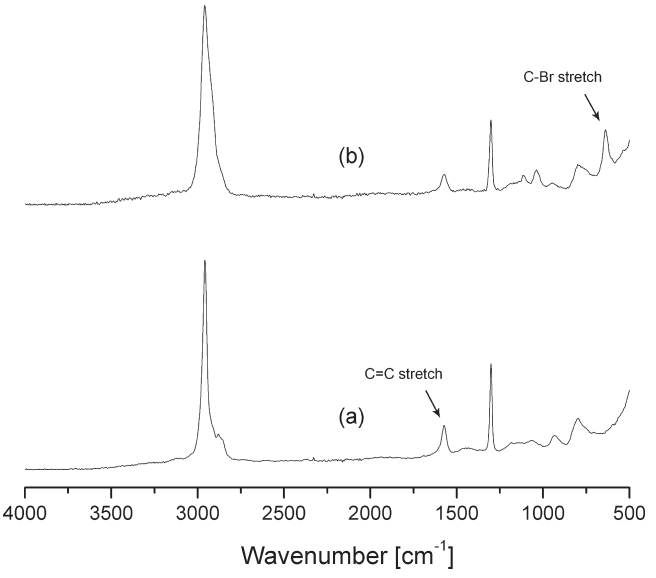

Figure 9. FT-Raman spectra of *E*-EBP (a) before and (b) after bromination.

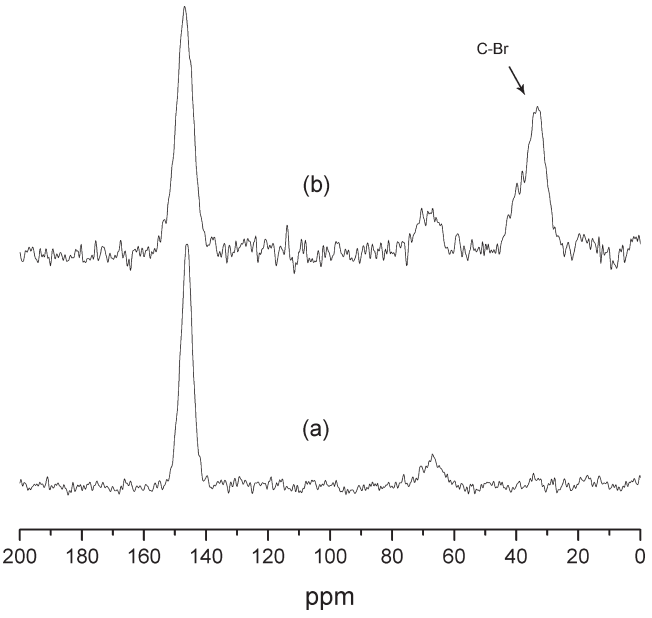

Figure 10. ^{13}C CP/MAS NMR spectra of *E*-EBP (a) before and (b) after bromination.

intense peak at 639 cm^{-1} is visible in spectrum (b), which can be assigned to the C−Br stretch vibration. A reduction of the peak at 1573 cm^{-1}, which can be assigned to the C=C stretch vibration, is also visible. In Figure 10, the ^{13}C CP MAS NMR spectra are given of *E*-EBP (a) before and (b) after bromination. In spectrum (b), the resonance at 34.4 ppm can be assigned to the C−Br organic groups.

By means of gravimetric analysis, the bromine accessibility of the surface ethene functionalities was investigated, as a function of reaction time. The bromine vapor reacts rapidly with the PMO ethene groups. After 30 min, the amount of brominated ethene functions is estimated at 1.7 per nm^2. After 60 and 120 min, 1.8 and 1.9 ethene functions per nm^2 are brominated, respectively. By further prolonging the reaction time, no significant increase in bromination is established. Via FT-Raman spectroscopy, the percentage of accessible C=C double bonds is estimated at approximately 30%. This was further confirmed by elementary analysis, which suggested that ca. 25% of the C=C double bonds are accessible to bromine.

Conclusions

The diastereoisomeric pure *E*-isomer of 1,2-bis-(triethoxysilyl)ethene, obtained using Grubbs' first generation catalyst, and the corresponding diastereoisomeric pure *E*-configured ethenylene-bridged PMOs were synthesized. The diastereoisomeric pure *Z*-isomer of 1,2-bis(triethoxysilyl)ethene was isolated for the first time and applied for the synthesis of *Z*-configured ethenylene-bridged PMOs. The use of the *E*-isomer of 1,2-bis-(triethoxysilyl)ethene, as supposed to the diastereoisomeric mixture, as a precursor for the synthsis of ethenylene-bridged PMOs enhances the structural ordering, the pore-size uniformity, and the hydrothermal stability. The changes in these properties were correlated with differences in the molecular level structure assessed by solid-state NMR spectroscopy.

Acknowledgment. The authors are indebted to the FWO-Vlaanderen (Fund for Scientific Research Flanders) and the University of Ghent for financial support.

Supporting Information Available: GC and ^{1}H-NMR of *E*-BTSE and *Z*-BTSE. Full characterization of Z-EBP (FT-Raman, XRD, ^{1}H−^{13}C CP/MAS NMR, and ^{1}H−^{29}Si CP/MAS NMR). ^{1}H−^{13}C CP/MAS kinetic curves for *E*-EBP, *Z*-EBP, vinyl-functionalized silica, and *Z*-EBO. ^{1}H−^{13}C CP/MAS NMR spectra of as-synthesized *E*-EBP and *Z*-EBP. ^{1}H−^{13}C CP/MAS kinetic curves for as-synthesized *E*-EBP and *Z*-EBP. ^{1}H−^{29}Si CP/MAS kinetic curves of *E*-EBP, 50(*E*,*Z*)-EBP, *Z*-EBP, and *Z*-EBO. Degree of framework condensation calculated using the areas obtained under Gausian fitting for *E*-EBP, 80(*E*,*Z*)-EBP, 50(*E*,*Z*)-EBP, *Z*-EBP, and *Z*-EBO. ^{1}H−^{13}C HECTOR NMR experiment of *Z*-EBO (PDF). This material is available free of charge via the Internet at http://pubs.acs.org.